A Comprehensive Load Flow Approach for Grid-connected and Islanded AC Microgrids

Evangelos E. Pompodakis, Georgios C. Kryonidis, *Member*, *IEEE*, and Minas C. Alexiadis, *Member*, *IEEE*

***Abstract*—This paper proposes a comprehensive load flow algorithm for balanced and unbalanced distribution systems considering the effect of a multi-grounded neutral conductor. The method is based on the implicit Z_{BUS} method presenting fast convergence and robustness regardless of the *R*/*X* ratio of the lines. Its distinct feature is its ability to handle all network configurations, including highly meshed distribution systems that operate in either islanded or grid-connected mode. Furthermore, an algorithm is proposed for overcoming the limitation of implicit Z_{BUS} method to treat PV nodes. Additionally, the concept of virtual impedance is incorporated into the proposed algorithm to accurately simulate the behavior of distributed generators (DGs) during the islanded operation. Numerical simulations are conducted in 33-Bus and 38-Bus balanced networks as well as in 25-Bus and 30-Bus unbalanced networks to verify the validity of the proposed load flow algorithm.**

***Index Terms*—Load flow, meshed distribution systems, multi-grounded systems, implicit Z_{BUS} method, islanded microgrids, PV nodes, virtual impedance**

NOMENCLATURE

I_{Lir}	Load current of node *i* at phase *r*={*a*, *b*, *c*}
V_{iy}	Voltage of node *i* at conductor *y*={*a*, *b*, *c*, *n*, *g*}
Z_{gri}	Grounding impedance at node *i*
Y_{ij}^{pz}	Self or mutual line admittance between nodes *i*-*j* and conductors {*p*, *z*}={*a*, *b*, *c*, *n*, *g*}
V_{irn}	Phase-to-neutral voltage of phase *r*={*a* ,*b*, *c*} at node *i*
P_{ir}	Active power of phase *r*={*a*, *b*, *c*} at node *i*
Q_{ir}	Reactive power of phase *r*={*a*, *b*, *c*} at node *i*
θ_{irn}	Angle of phase-to-neutral voltage of phase *r*={*a*, *b*, *c*} at node *i.*
f	Frequency of the network
f_{0i}	Nominal frequency applied to the droop equation
V_{0i}	Nominal voltage applied to the droop equation
K_{Qi}	Voltage droop gain
K_{Pi}	Frequency droop gain
P_{Gi}	*A*ctive power of DG *i* determined by the droop equation
Q_{Gi}	*R*eactive power of DG *i* determined by the droop equation
V_{Gi}	*T*erminal voltage of DG *i*
P_{slack}	Active power flowing through the virtual slack bus
$I_{pos,i}$	Positive sequence current of synchronous generator (SG) *i*
$I_{neg,i}$	Negative sequence current of SG *i*
$I_{zero,i}$	Zero sequence current of SG *i*
$V_{pos,i}$	Positive sequence voltage of SG *i*
$V_{neg,i}$	Negative sequence voltage of SG *i*
$V_{zero,i}$	Zero sequence voltage of SG *i*
$Y_{neg,i}$	Negative sequence internal admittance of SG *i*
$Y_{zero,i}$	Zero sequence internal admittance of SG *i*
$V_{y(vir)}$	Virtual slack bus voltage at conductor *y*={a, b, c, n, g}
$Z_{y(vir)}$	Impedance of virtual slack bus at conductor *y*={a, b, c, n, g}
$V_{virtual,i}$	Virtual voltage of DG *i*
Z_{vi}	Virtual impedance of DG *i*
I_{Gi}	Feedback current of DG *i*

«This research is co-financed by Greece and the European Union (European Social Fund- ESF) through the Operational Programme «Human Resources Development, Education and Lifelong Learning» in the context of the project "Strengthening Human Resources Research Potential via Doctorate Research" (MIS-5000432), implemented by the State Scholarships Foundation (IKY)». The authors are with the School of Electrical and Computer Engineering, Aristotle University of Thessaloniki, Thessaloniki GR 54124, Greece (e-mail: bobodakis@hotmail.com; kryonidi@ece.auth.gr; minalex@auth.gr).

I. INTRODUCTION

Due to the high penetration of distributed generators (DGs) in medium- (MV) and low-voltage (LV) networks, several technical problems have emerged such as overvoltage, unbalance, harmonics, and overloading of the existing equipment [1]. In reality, loads are never perfectly balanced and the grounding resistances of LV networks vary practically from 1 Ohm to several tens of Ohms [2], resulting in significant neutral-to-ground voltages and imbalance between the phases. The problem was exacerbated over the last decades by the connection of single-phase DGs into the LV network. As a result, the assumption of balanced LV networks, which has been commonly adopted by many studies in literature, may not be realistic. Therefore, to accurately estimate the operation of LV networks, load flow models should explicitly consider the neutral conductor as well as the multiple grounding of the neutral conductors. The significance of neutral and grounding conductors towards the load flow analysis of four-wire networks is extensively analyzed in [3] and [4].

Several studies have been carried out in the past to calculate the load flow in grid-connected systems. In [5], a method based on the implicit Z_{BUS} is proposed. However, it does not explicitly consider the neutral conductor and grounding resistances. Furthermore, it can be applied only in networks with PQ buses due to its inherent difficulty to handle PV nodes [6]. The authors in [7] and [8] consider the neutral conductor and ground using the Backward-Forward Sweep (BFS) method. However, the BFS method can only be applied in radial configurations. A Newton–Raphson (NR)-based method is proposed in [9], which includes into calculations the neutral conductor. Nonetheless, it often fails to converge for highly unbalanced LV networks with high *R*/*X* ratio [10], while the convergence is vulnerable to the initial selected voltage values, as usually occurs with all NR-based methods.

Citation Information: DOI: 10.1109/TPWRS.2019.2945011

Conventional load flow methods are inapplicable in islanded microgrids (MGs) for two main reasons. First, there is no such a large DG unit to undertake the role of a slack bus to keep the voltage and frequency of the MG constant. Secondly, the DGs are not represented as PV/PQ nodes but their operation is usually determined from their droop equations. To calculate the load flow in islanded MGs, authors in [11], [12] and [13] propose three methods based on BFS. However, they can be applied to networks with only a radial configuration. In [14] and [15], the classic NR method is modified to accommodate the particular properties of islanded MGs. In [16], the Gauss-Seidel (GS) method is adjusted to solve the load flow problem (LFP) in islanded MGs. Finally, the authors in [17] propose a matrix-inversion-free method based on particle swarm optimization with fast computation time and robust implementation, while in [18], a new methodology is proposed according to which the voltage of the slack bus and the frequency are iteratively adjusted to nullify the apparent power flowing through the slack bus. However, all the above-mentioned methods assume a balanced network limiting their applicability in asymmetrical networks.

Some other approaches have been presented in literature to simulate the operation of islanded MGs by including the network asymmetries. More specifically, a load flow approach based on the distributed slack bus model is proposed in [19]. However, the concept of distributed slack bus does not reflect the real behavior of a droop-controlled islanded microgrid [15]. In [20], a three-phase load flow approach is proposed to simulate the transient phenomenon of synchronous generators in islanded MGs considering a slack bus relaxation. Nevertheless, it cannot be applied in real-time applications, where the main interest is the steady-state condition of the network, due to its long execution time. Finally, the authors in [21] propose a solution based on the Newton-trust region method for unbalanced MGs. However, the neutral and grounding conductors are neglected, while the time complexity is equal to $O(n^3)$ limiting its applicability in real time applications.

In droop-controlled LV islanded MGs, virtual impedance loops are often adopted in combination with the conventional droop equations of DG units. Virtual impedances are applied to DGs for two main reasons: first, to decouple real and reactive power in LV networks with high R/X ratio, and second, to improve the accuracy of reactive power-sharing between the DGs in islanded MGs. None of the above-referred papers dealing with the LFP in islanded MGs has taken the concept of virtual impedance into consideration. The influence of virtual impedance on the LFP calculations is studied for the first time in [22] and [23], where it is concluded that the neglect of virtual impedance from the LFP leads to misleading results. Nevertheless, a balanced distribution system is assumed, neglecting the network asymmetries.

This paper has two main objectives. The first one is to develop a comprehensive load flow approach for islanded and grid-connected MGs, considering explicitly the neutral and grounding. The proposed approach can be applied in all kinds of configurations, including highly meshed MGs, regardless of the R/X ratio of the lines. It presents fast convergence, low computation time, high accuracy, and robustness. The second objective is to integrate into the load flow model the concept of virtual impedance, which is often adopted by the controllers of droop-controlled DGs in islanded MGs.

The rest of the paper is organized as follows. The proposed load flow approach for grid-connected networks is analyzed in Section II. In the same section, a procedure is proposed to enable the implicit Z_{BUS} method to handle networks with an unlimited number of PV nodes. In Section III, an algorithm is presented to solve the LFP in balanced and unbalanced droop-controlled islanded MGs. The concept of virtual impedance in both balanced and unbalanced islanded MGs is studied in Section IV. Finally, the numerical validation of the algorithm and an investigation study are provided in Sections V and VI, respectively, while Section VII concludes the paper.

II. Proposed Method for Grid-connected Networks

In this section, the implementation of the proposed approach in grid-connected unbalanced networks is described. Initially, the implicit Z_{BUS} method of [5] is modified to incorporate the neutral and grounding of LV networks. Subsequently, a method is developed to overcome the inherent difficulty of implicit Z_{BUS}-based methods to model PV nodes [6]. Thus, the section is divided into two separate parts. In the first part, the proposed load flow approach considering the neutral and grounding is introduced in a network with PQ nodes. In the second part, the method for modeling PV nodes is analytically described.

A. Networks with only PQ Nodes

The full configuration of an unbalanced LV network is presented in Fig. 1a, including the neutral conductor and the grounding resistance. Let us define the current and voltage vectors of node i as follows:

$$\boldsymbol{I_i} = \left[I_{Lia},\ I_{Lib},\ I_{Lic},\ (V_{in}-V_{ig})/Z_{gri}-I_{Lia}-I_{Lib}-I_{Lic},\ -(V_{in}-V_{ig})/Z_{gri} \right]^T \quad (1)$$

$$\boldsymbol{V_i} = \left[V_{ia},\ V_{ib},\ V_{ic},\ V_{in},\ V_{ig} \right]^T \quad (2)$$

where I_{Lir} and V_{iy} denote the load current and voltage (in complex form) of node i at phase $r=\{a, b, c\}$ and conductor $y=\{a, b, c, n, g\}$, respectively. For a network with m nodes, the load vectors can be expressed as a function of the voltage vectors according to (3).

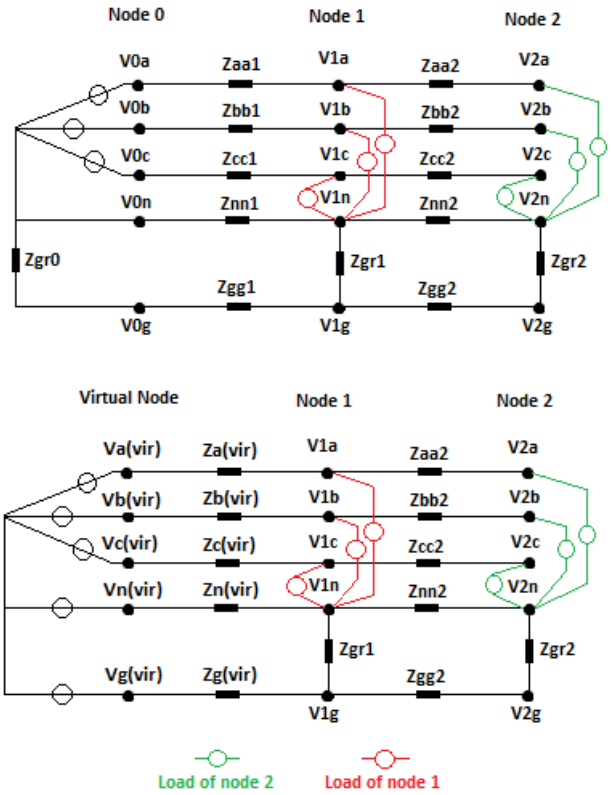

Fig. 1. From Top to Bottom: a) Equivalent circuit of a grid-connected network, consisting of the slack node (Node 0) and two load nodes. b) Equivalent circuit of an islanded MG, consisting of the virtual slack node with the virtual slack impedances and two load nodes.

$$\begin{bmatrix} \boldsymbol{I_0} \\ \boldsymbol{I_1} \\ \dots \\ \boldsymbol{I_m} \end{bmatrix} = \begin{bmatrix} \boldsymbol{Y_{00}} & \boldsymbol{Y_{01}} & \cdots & \boldsymbol{Y_{0m}} \\ \boldsymbol{Y_{10}} & \boldsymbol{Y_{11}} & \cdots & \boldsymbol{Y_{1m}} \\ \vdots & \vdots & \cdots & \vdots \\ \boldsymbol{Y_{m0}} & \boldsymbol{Y_{m1}} & \cdots & \boldsymbol{Y_{mm}} \end{bmatrix} \cdot \begin{bmatrix} \boldsymbol{V_0} \\ \boldsymbol{V_1} \\ \dots \\ \boldsymbol{V_m} \end{bmatrix} \tag{3}$$

Here, each non-diagonal element of the admittance matrix in (3), e.g. $\boldsymbol{Y_{ij}}$ *for* $i \neq j$, is defined by (4), which includes the self- and mutual admittances of each line sector between the nodes i and j. The diagonal elements of (3) are defined as: $\boldsymbol{Y_{ii}} = -\sum_{k=0}^{i-1}(\boldsymbol{Y_{ik}}) - \sum_{k=i+1}^{m}(\boldsymbol{Y_{ik}})$.

$$\boldsymbol{Y_{ij}} = \begin{bmatrix} Y_{ij}^{aa} & Y_{ij}^{ab} & Y_{ij}^{ac} & Y_{ij}^{an} & Y_{ij}^{ag} \\ Y_{ij}^{ba} & Y_{ij}^{bb} & Y_{ij}^{bc} & Y_{ij}^{bn} & Y_{ij}^{bg} \\ Y_{ij}^{ca} & Y_{ij}^{cb} & Y_{ij}^{cc} & Y_{ij}^{cn} & Y_{ij}^{cg} \\ Y_{ij}^{na} & Y_{ij}^{nb} & Y_{ij}^{nc} & Y_{ij}^{nn} & Y_{ij}^{ng} \\ Y_{ij}^{ga} & Y_{ij}^{gb} & Y_{ij}^{gc} & Y_{ij}^{gn} & Y_{ij}^{gg} \end{bmatrix} \tag{4}$$

To formulate the final equations that are subject to the iterative process of the LFP solution, the first four rows of (3) are completely eliminated and (5) is obtained.

$$\begin{bmatrix} I'_0 \\ \boldsymbol{I_1} \\ \dots \\ \boldsymbol{I_m} \end{bmatrix} = \begin{bmatrix} \boldsymbol{Y'_{00}} & \boldsymbol{Y'_{01}} & \cdots & \boldsymbol{Y'_{0m}} \\ \boldsymbol{Y_{10}} & \boldsymbol{Y_{11}} & \cdots & \boldsymbol{Y_{1m}} \\ \vdots & \vdots & \cdots & \vdots \\ \boldsymbol{Y_{m0}} & \boldsymbol{Y_{m1}} & \cdots & \boldsymbol{Y_{mm}} \end{bmatrix} \cdot \begin{bmatrix} \boldsymbol{V_0} \\ \boldsymbol{V_1} \\ \dots \\ \boldsymbol{V_m} \end{bmatrix} \tag{5}$$

This elimination occurs because the first four rows of $\boldsymbol{I_0}$ are dependent on the currents injected from the slack bus, namely I_{L0a}, I_{L0b}, and I_{L0c}, which are all unknown, in contrast to the elements of the other current vectors, which can be iteratively calculated depending on the type of load and the phase voltages of the previous iteration. The size of $\boldsymbol{Y'_{ij}}$ is 1x5 and includes the self- and mutual admittance of the ground conductor, i.e., the last row of (4). The next step is to move the voltage variables of the current vectors, as expressed in (1), to the right side of (5) as follows:

$$\boldsymbol{I_{new}} = \boldsymbol{Y_{new}} \cdot \boldsymbol{V} \tag{6}$$

where $\boldsymbol{V}$ is the vector $[\boldsymbol{V_0}, \boldsymbol{V_1}, \dots, \boldsymbol{V_m}]^{\mathrm{T}}$ consisting of network voltages, while $\boldsymbol{Y_{new}}$ is the modified admittance matrix. $\boldsymbol{I_{new}}$ contains only the load current variables defined in (1).

As a last step, we define the final matrices $\boldsymbol{Y'_{fin}}$ and $\boldsymbol{Y_{fin}}$. The first one consists of the first four columns of $\boldsymbol{Y_{new}}$, while the second one consists of the remaining columns so that $\boldsymbol{Y_{new}} = [\boldsymbol{Y'_{fin}}\ \boldsymbol{Y_{fin}}]$. Equation (7) is derived from (6) by removing the product $\boldsymbol{Y'_{fin}} \cdot [V_{0a}, V_{0b}, V_{0c}, V_{0n}]^{\mathrm{T}}$ from both equation sides. Using (7), we finally derive (8), which is iteratively solved until a certain preset tolerance is reached.

$$-\boldsymbol{Y'_{fin}} \cdot \begin{bmatrix} V_{0a} \\ V_{0b} \\ V_{0c} \\ V_{0n} \end{bmatrix} + \boldsymbol{I_{new}} = -\boldsymbol{Y'_{fin}} \cdot \begin{bmatrix} V_{0a} \\ V_{0b} \\ V_{0c} \\ V_{0n} \end{bmatrix} + \boldsymbol{Y_{new}} \cdot \boldsymbol{V} \tag{7}$$

$$\boldsymbol{Y_{fin}}^{-1} \cdot \left(-\boldsymbol{Y'_{fin}} \cdot \begin{bmatrix} V_{0a} \\ V_{0b} \\ V_{0c} \\ V_{0n} \end{bmatrix} + \begin{bmatrix} 0 \\ I_{L1a} \\ I_{L1b} \\ I_{L1c} \\ -I_{L1a} - I_{L1b} - I_{L1c} \\ 0 \\ \vdots \\ I_{Lma} \\ I_{Lmb} \\ I_{Lmc} \\ -I_{Lma} - I_{Lmb} - I_{Lmc} \\ 0 \end{bmatrix}^{k} \right) = \begin{bmatrix} V_{0g} \\ V_{1a} \\ V_{1b} \\ V_{1c} \\ V_{1n} \\ V_{1g} \\ \vdots \\ V_{ma} \\ V_{mb} \\ V_{mc} \\ V_{mn} \\ V_{mg} \end{bmatrix}^{k+1} \tag{8}$$

According to (8), all the unknown voltages of the network are iteratively calculated. The variable k is the iteration number. The vector $[V_{0a}, V_{0b}, V_{0c}, V_{0n}]^{\mathrm{T}}$ expresses the slack bus, which is a constant reference point, while $\boldsymbol{Y'_{fin}}$ and $\boldsymbol{Y_{fin}}$ consist of constant values. Thus, contrary to NR-based methods, no recalculation of these matrices is needed in each iteration, saving significant calculation time. Finally, the values of single-phase load currents are calculated in each iteration according to [8, Table I] based on the type of load, e.g. constant power, impedance or current.

B. Modeling of PV nodes

Implicit Z_{BUS} method has comparable convergence properties with the NR method, when the only voltage-specified node of the network is the slack bus. However, it is not applicable to networks with at least one PV node since it suffers from divergence issues [6]. To make the implicit Z_{BUS} method also applicable in networks with unlimited number of PV nodes, a method is proposed that estimates in every iteration the required power produced by each phase of PV nodes.

Firstly, the complex power equation of phase r of PV node i is calculated as follows:

$$S_{ir} = (V_{ir} - V_{in}) \cdot \sum_{N=1}^{N_t} \sum_{k\in\{a,b,c,n,g\}} (V_{Nk} - V_{ik})^* \cdot Y^*_{iN}{}^{rk} \quad (9)$$

S_{ir} is the complex apparent power of PV node i of phase r. V_{iy} is the complex voltage of node i of conductor y, while $Y^*_{ij}{}^{pz}$ is the conjugate complex admittance of the line between the nodes i and j and conductors p and z ($\{p, z\} = \{ a, b, c, n, g \}$). N_t is the total number of network nodes. Subsequently, all the phase voltages of PV nodes in (9) need to be written as a function of the phase-to-neutral voltage as follows:

$$V_{ir} = V_{irn} + V_{in} \quad (10)$$

where V_{irn} is the voltage between the phase r and the neutral at the node i. This modification is necessary because the following sensitivity matrix is constructed with all voltages expressed with respect to the neutral conductor and not to the reference point, i.e., the neutral point of slack bus. After the modification, (9) is subsequently separated into real and imaginary parts and takes the form shown in (11).

$$S_{ia} = P_{ia} + Q_{ia} \cdot j \quad (11a)$$

$$S_{ib} = P_{ib} + Q_{ib} \cdot j \quad (11b)$$

$$S_{ic} = P_{ic} + Q_{ic} \cdot j \quad (11c)$$

The deviation of the voltage magnitudes, e.g. $|V_{ian}|$, and angles of each PV node i from their specified values ($[\cdot]^{sp}$) at each iteration k are calculated by (12a). The voltage angle difference between the three phases of each PV node was selected to be 120^o to represent the case of PV nodes with symmetrical voltage, namely equal magnitudes and angles shifted by 120^o from each other. The calculated deviations of (12a) are applied in (12b) so that the required variation of the reactive power of phases (a, b, c) and the active power of phases (b, c) are calculated. It is worth noticing that the derivatives of the square matrix of (12b) are derived from (11). The sparse matrix of (12b) results from the strong coupling between P-V and Q-θ due to the high R/X ratio of LV systems. Its structure could be modified for different R/X ratios.

$$\begin{bmatrix} d|V_{ian}| \\ d|V_{ibn}| \\ d|V_{icn}| \\ d\theta_{ibn} \\ d\theta_{icn} \end{bmatrix}^k = \begin{bmatrix} |V_{ian}| \\ |V_{ibn}| \\ |V_{icn}| \\ -120^o \\ 120^o \end{bmatrix}^{sp} - \begin{bmatrix} |V_{ian}| \\ |V_{ibn}| \\ |V_{icn}| \\ (\theta_{ibn} - \theta_{ian}) \\ (\theta_{icn} - \theta_{ian}) \end{bmatrix}^k \quad (12a)$$

$$\begin{bmatrix} dQ_{ia} \\ dQ_{ib} \\ dQ_{ic} \\ dP_{ib} \\ dP_{ic} \end{bmatrix}^k = \begin{bmatrix} \frac{\partial Q_{ia}}{\partial |V_{ian}|} & 0 & 0 & 0 & 0 \\ 0 & 0 & 0 & \frac{\partial Q_{ib}}{\partial \theta_{ibn}} & 0 \\ 0 & 0 & 0 & 0 & \frac{\partial Q_{ic}}{\partial \theta_{icn}} \\ 0 & \frac{\partial P_{ib}}{\partial |V_{ibn}|} & 0 & 0 & 0 \\ 0 & 0 & \frac{\partial P_{ic}}{\partial |V_{icn}|} & 0 & 0 \end{bmatrix}^k \cdot \begin{bmatrix} d|V_{ian}| \\ d|V_{ibn}| \\ d|V_{icn}| \\ d\theta_{ibn} \\ d\theta_{icn} \end{bmatrix}^k \quad (12b)$$

$$\begin{bmatrix} Q_{ia} \\ Q_{ib} \\ Q_{ic} \\ P_{ib} \\ P_{ic} \end{bmatrix}^{k+1} = \begin{bmatrix} Q_{ia} \\ Q_{ib} \\ Q_{ic} \\ P_{ib} \\ P_{ic} \end{bmatrix}^k + \lambda \cdot \begin{bmatrix} dQ_{ia} \\ dQ_{ib} \\ dQ_{ic} \\ dP_{ib} \\ dP_{ic} \end{bmatrix}^k \quad (12c)$$

$$P_{ia}{}^{k+1} = (P_i^{sp} - P_{ib}{}^{k+1} - P_{ic}{}^{k+1}) \quad (12d)$$

The estimated values of reactive power of phases (a, b, c) and active power of phases (b, c) are calculated for the next iteration (k+1) from (12c) using the results of (12b). The estimated active power of phase a is calculated by (12d), so that the constraint of specified three-phase power (P_i^{sp}) is fulfilled. Coefficient λ is introduced in (12c) to improve the stability of the iterative process. Low values of λ result in slower convergence characteristics but the algorithm becomes more stable and the convergence is highly guaranteed [24]. On the other hand, very high values of the coefficient can even lead to calculation divergence. A flowchart of the proposed method is shown in Fig. 2, where the voltage of every conductor of all the nodes is calculated from (8) using the estimated PV node power values of (12). The algorithm terminates if the difference of all voltage values between two subsequent iterations is smaller than a pre-defined tolerance (ε).

III. Proposed Method for Droop-controlled Islanded Microgrids

In this section, we propose a new approach based on the virtual slack node concept that enables the method presented in Section II to be applicable in islanded MGs. The proposed method can be applied in both balanced and unbalanced islanded MGs.

In the next subsections, the theoretical background of the islanded MG operation is initially presented. Afterward, the virtual slack node concept is described. Finally, the last two subsections are devoted to the balanced and unbalanced operation of the islanded MG.

A. Theoretical Background of Islanded MGs

During the islanded operation of MG, DGs operate in a droop control mode to proportionally share the active and reactive power demand. The generated active and reactive powers of DGs are determined by the well-known P-f and Q-V droop curves [21] expressed by:

$$P_{Gi} = \frac{f_{0i} - f}{K_{Pi}} \quad (13a)$$

$$Q_{Gi} = \frac{|V_{0i}| - |V_{Gi}|}{K_{Qi}} \quad (13b)$$

where f, f_{0i}, K_{pi}, P_{Gi}, V_{Gi}, V_{0i}, K_{Qi} and Q_{Gi} are the output frequency, nominal frequency, frequency droop gain, active power output, output voltage magnitude, nominal voltage, voltage droop gain and reactive power output of DG i, respectively.

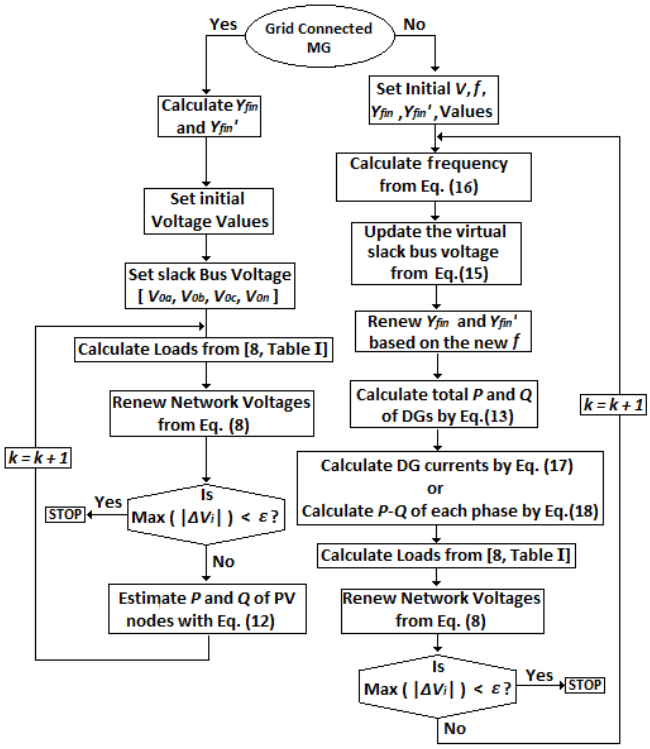

Fig. 2. Flowchart of the proposed algorithm for grid-connected and droop controlled islanded MGs

B. *The Concept of Virtual Slack Node for Solving the Load Flow in Balanced and Unbalanced Islanded MGs*

Firstly, we assume that the islanded MG has a virtual slack node (consisting of virtual slack sources e.g., $V_{a(vir)}$ in Fig. 1b), which is connected in a random node of the network through a freely selected impedance (e.g., $Z_{a(vir)}$ in Fig. 1b). In fact, we add one more node in a random place of the network acting as a slack bus in the mathematical calculations. The active power flowing through the slack node ($P_{slack}^{\ k}$) is calculated in every iteration k from (14):

$$P_{slack}^{\ k} = real\left(\begin{bmatrix} \frac{V_{a(vir)}}{Z_{a(vir)}^{\ *}} & \frac{V_{b(vir)}}{Z_{b(vir)}^{\ *}} & \frac{V_{c(vir)}}{Z_{c(vir)}^{\ *}} & \frac{V_{n(vir)}}{Z_{n(vir)}^{\ *}} & \frac{V_{g(vir)}}{Z_{g(vir)}^{\ *}} \end{bmatrix} \begin{bmatrix} (V_{1a} - V_{a(vir)}) \\ (V_{1b} - V_{b(vir)}) \\ (V_{1c} - V_{c(vir)}) \\ (V_{1n} - V_{n(vir)}) \\ (V_{1g} - V_{g(vir)}) \end{bmatrix}^{*} \right)^{k} \tag{14}$$

According to the proposed method, $P_{slack}^{\ k}$ is allocated in every iteration k to DGs of the network based on the characteristics of the corresponding droop curves. Thus, after a number of iterations, the active power of virtual slack node is forced to zero.

Furthermore, the voltage of the virtual slack node is equalized at the beginning of each new iteration (k+1) with the voltage of its adjacent node, as it was calculated in the last iteration k as expressed by (15):

$$\begin{bmatrix} V_{a(vir)} \\ V_{b(vir)} \\ V_{c(vir)} \\ V_{n(vir)} \\ V_{g(vir)} \end{bmatrix}^{k+1} = \begin{bmatrix} V_{1a} \\ V_{1b} \\ V_{1c} \\ V_{1n} \\ V_{1g} \end{bmatrix}^{k} \tag{15}$$

After the algorithm has converged, the slack node and the directly connected adjacent node have acquired the same voltage. Thus, the current flowing through the impedances $Z_{y(vir)}$ is forced to zero, resulting in zero active and reactive power at the virtual slack bus. In this way, the virtual slack node does not influence the network and it is as if it does not exist. It is pointed out that (14) and (15) are referred to an unbalanced network but they can be easily applied also in balanced networks of one phase by using only the first elements of the matrices in (14) and (15). With the concept of virtual slack bus, the mathematical formulations of load flow problem in islanded MGs are the same as in grid-connected networks since the virtual slack node is treated mathematically as a real slack node. Thus, the same concept can also be applied in other load flow solvers, e.g., NR, GS, BFS.

C. *Balanced Islanded Microgrids*

In balanced networks, we consider only the one phase since the voltage of the neutral conductor is zero. First, we define a virtual slack bus as explained in the previous subsection. Subsequently, the MG frequency is updated based on the active power flowing through the virtual slack node, which is calculated by (14), as follows:

$$df^{k} = \frac{P_{slack}^{\ k}}{\sum_{i=1}^{m_{dr}} \frac{1}{K_{pi}}} \tag{16a}$$

$$f^{k+1} = f^{k} + df^{k} \tag{16b}$$

where m_{dr} is the total number of droop-controlled DGs. An acceleration factor in (16b) can further improve the convergence speed of the algorithm as explained in Appendix A. With the new updated MG frequency, we calculate the generated active power of each DG using (13a). In this way, the active power flowing through the slack node is nullified after a number of iterations since it is distributed among the DGs. Additionally, $\boldsymbol{Y'_{fin}}$ and $\boldsymbol{Y_{fin}}$ are recalculated at every iteration based on the new MG frequency.

The reactive power of each DG for the next iteration is determined from (13b), depending on the voltage of the respective node as calculated at the last iteration. From the author's experience, the convergence and stability of the algorithm can be improved if we also consider the reactive power of DG of the previous iteration as shown in (A2) of Appendix A. In this way, we can avoid large voltage oscillations arising from the large variation of DG-reactive powers.

D. *Unbalanced Islanded Microgrids*

Similar to the balanced systems, the MG frequency at every new iteration is calculated from (16), where $P_{slack}^{\ k}$ is calculated according to (14). The positive sequence active power of DGs is calculated at every iteration from (13a) based on the frequency value of (16). The positive sequence reactive power of DGs is calculated from (13b). Please note

that in (13b) the positive sequence component of the unbalanced DG voltage (V_{Gi}) is applied [25].

Depending on the control strategy adopted, the current and voltage of each DG in an unbalanced MG can be simulated according to the following operation modes [26]:
a) The DG-generated current is balanced (only positive sequence), while the generated voltage is unbalanced.
b) Both the DG-generated current and voltage are unbalanced.
c) The DG-generated voltage is balanced [21], [25], [27], while its current is unbalanced.

In the first two operation modes, the phase currents are simply calculated by the composition of the sequence components and are subsequently introduced in (8). More specifically, the positive sequence current component is usually determined from (17a) using the powers of (13). The negative and zero sequence current components are dependent on the adopted control strategy. As an example, the authors in [25] adopt a control strategy, according to which the negative and zero sequence current of the DGs are linearly related to their negative and zero sequence voltage, respectively. The same relation between negative and zero sequence current and voltage occurs in synchronous generators as well due to their internal negative and zero sequence admittances ($Y_{neg,i}$, $Y_{zero,i}$) [26]. In that case, the negative and zero sequence current components are specified from the voltage sequence components, as calculated in the previous iteration, according to (17b) and (17c).

$$I_{pos,i}^{k+1} = \frac{1}{3} \cdot \left(\frac{P_i^{k+1} + Q_i^{k+1}}{V_{pos,i}^{k}} \right)^{*} \tag{17a}$$

$$I_{neg,i}^{k+1} = Y_{neg,i} \cdot V_{neg,i}^{k} \tag{17b}$$

$$I_{zero,i}^{k+1} = Y_{zero,i} \cdot V_{zero,i}^{k} \tag{17c}$$

In the third operation mode, the phase-to-neutral voltage magnitude of phases *b* and *c* should track at each iteration *k* the magnitude of phase *a*, while the angle deviation of phase *b* and *c* from phase *a* must track -120° and 120°, respectively. The estimated active and reactive power deviation of phase *b* and *c* are expressed by (18b) using the voltage and angle deviation values of (18a). The square matrix of (18b) has been simplified because of the weak coupling between *P*-θ and *Q*-*V*, resulting from the high *R*/*X* ratio of LV grids. The reactive and active powers of phase *b* and *c* are updated at each iteration for DG *i* according to (18c). Finally, the reactive and active powers of phase *a* are calculated from (18d) so that the total three-phase power produced from DG *i* at iteration *k*+1 is equal to the specified values (Q_i^{sp}, P_i^{sp}) resulting from droop equations (13).

$$\begin{bmatrix} d|V_{ibn}| \\ d|V_{icn}| \\ d\theta_{ibn} \\ d\theta_{icn} \end{bmatrix}^{k} = \begin{bmatrix} |V_{ian}| \\ |V_{ian}| \\ -120^{o} \\ 120^{o} \end{bmatrix}^{sp} - \begin{bmatrix} |V_{ibn}| \\ |V_{icn}| \\ (\theta_{ibn} - \theta_{ian}) \\ (\theta_{icn} - \theta_{ian}) \end{bmatrix}^{k} \tag{18a}$$

$$\begin{bmatrix} dQ_{ib} \\ dQ_{ic} \\ dP_{ib} \\ dP_{ic} \end{bmatrix}^{k} = \begin{bmatrix} 0 & 0 & \frac{\partial Q_{ib}}{\partial \theta_{ibn}} & 0 \\ 0 & 0 & 0 & \frac{\partial Q_{ic}}{\partial \theta_{icn}} \\ \frac{\partial P_{ib}}{\partial |V_{ibn}|} & 0 & 0 & 0 \\ 0 & \frac{\partial P_{ic}}{\partial |V_{icn}|} & 0 & 0 \end{bmatrix}^{k} \cdot \begin{bmatrix} d|V_{ibn}| \\ d|V_{icn}| \\ d\theta_{ibn} \\ d\theta_{icn} \end{bmatrix}^{k} \tag{18b}$$

$$\begin{bmatrix} Q_{ib} \\ Q_{ic} \\ P_{ib} \\ P_{ic} \end{bmatrix}^{k+1} = \begin{bmatrix} Q_{ib} \\ Q_{ic} \\ P_{ib} \\ P_{ic} \end{bmatrix}^{k} + \lambda \cdot \begin{bmatrix} dQ_{ib} \\ dQ_{ic} \\ dP_{ib} \\ dP_{ic} \end{bmatrix}^{k} \tag{18c}$$

$$\begin{bmatrix} Q_{ia} \\ P_{ia} \end{bmatrix}^{k+1} = \begin{bmatrix} Q_i \\ P_i \end{bmatrix}^{sp} - \begin{bmatrix} Q_{ib} + Q_{ic} \\ P_{ib} + P_{ic} \end{bmatrix}^{k+1} \tag{18d}$$

Knowing the powers (from (18)) or directly the currents (from (17)) of each DG, we can calculate the voltages from (8). A flowchart of the proposed method is illustrated in Fig. 2. The voltage sources of the virtual slack bus are equalized at the beginning of each new iteration with them of the adjacent node according to (15).

IV. The Concept of Virtual Impedance in Droop-controlled Islanded Microgrids

To decouple real and reactive power, to increase the stability margin, and to improve the reactive power sharing between DGs, virtual impedance loops are often adopted in combination with the conventional droop control. The majority of existing studies in literature completely ignore the virtual impedance from the load flow calculations, resulting in inaccurate results [22], [23]. In this section, the concept of virtual impedance and its integration in the proposed steady-state load flow method is presented for balanced and unbalanced systems.

A. Balanced Islanded Microgrids

By considering the virtual impedance at the control of DG unit, the operation of DG unit is described by (19), where $V_{virtual,i}$ is the virtual voltage of DG unit *i* and Z_{vi} the virtual impedance, I_{Gi} and V_{Gi} are the feedback current and the generated voltage, respectively, of the DG unit *i*. A more detailed analysis about the concept of virtual impedance is out of the scope of this paper since in this work we are interested only in the integration of the virtual impedance into the steady-state load flow model.

$$\left|V_{virtual,i}\right| = \left|V_{0i}\right| - K_{Qi} \cdot Q_{Gi} \tag{19a}$$

$$V_{Gi} = V_{virtual,i} - I_{Gi} \cdot Z_{vi} \tag{19b}$$

To consider the virtual impedance of DG unit *i* into the load flow calculations, we add into the system an additional node, which is connected to the DG node *i* through the virtual impedance (Z_{vi}). Let us assume that the network consists of a set of *N* nodes, where N_{VIR} of them represent nodes with DG units that are controlled with virtual impedances, such that $N_{VIR} \subseteq N$. At any node $i \in N_{VIR}$, an additional node $j \in N_{ADD}$ is connected through an impedance $Z_{v(ij)}$ (its value equals to the virtual one), where N_{ADD} is the

set of all additional nodes connected into the network. Obviously, the number of nodes belonging to N_{ADD} is equal to that of N_{VIR}, as every additional node corresponds with a virtual impedance-controlled DG. Afterwards, the load flow equation system is reconstructed to include $N+N_{add}$ nodes.

The following steps are subsequently applied to solve the LFP, taking into consideration the virtual impedance control of DG units:

Step 1: *Calculate the load flow for $N+N_{add}$ nodes and take the voltage values.*
Step 2: *The reactive power of node $i \in N_{VIR}$ is calculated by (13b), from the voltage of the node $j \in N_{ADD}$, which is connected through the impedance $Z_{v(ij)}$. The active power of node $i \in N_{VIR}$ is calculated by (13a) from the system frequency.*
Step 3: *Calculate the currents of all the nodes $n \in N$ from their apparent powers S_n and voltages V_n.*
Step 4: *Set $I_j=I_i$ and $I_i=0$ for every set of Nodes $i, j \in N_{VIR}, N_{ADD}$.*
Step 5: *Go to step 1 and repeat until the final convergence of the algorithm.*

B. Unbalanced Islanded Microgrids

In case of an unbalanced MG, droop equations (see (13)) can be used but only for the positive sequence components [25]. The negative and zero sequence current components are dependent on the control strategy adopted, as explained in Section III-D. The process of solving the LFP in unbalanced networks considering the virtual impedance of DGs is similar than that of balanced systems, with the exception that the negative and zero sequence current components need to be considered. Again, an additional node $j \in N_{ADD}$ needs to be connected to any node $i \in N_{VIR}$ through an impedance that is equal to the value of the virtual one. The following steps describe the algorithm:

Step 1: *Calculate the load flow for $N+N_{add}$ nodes and take the voltage values.*
Step 2: *The positive sequence reactive power of node $i \in N_{VIR}$ is calculated by (13b), from the positive sequence voltage of the node $j \in N_{ADD}$, which is connected through the impedance $Z_{v(ij)}$ with. The positive sequence active power is calculated by (13a) from the system frequency.*
Step 3: *Calculate the positive sequence current of each node $i \in N_{VIR}$ from its positive sequence apparent power (calculated at step 2) and voltage (calculated at step 1).*
Step 4: *Calculate the negative and zero sequence current of each node $i \in N_{VIR}$, depending on the adopted control strategy of each DG and the voltage values of step 1.*
Step 5: *Compose the current of each node $i \in N_{VIR}$ based on the sequence components of the two previous steps.*
Step 6: *Calculate the currents of all the other nodes $n \in N \setminus N_{VIR}$ of the network from their apparent power S_n (specified for PQ nodes) and the voltage V_n (calculated at step 1).*
Step 7: *Set $I_j=I_i$ and $I_i=0$ for every set of Nodes $(i, j) \in (N_{VIR}, N_{ADD})$.*
Step 8: *Go to step 1 and repeat until the final convergence of the algorithm.*

V. Algorithm Validation

In this section, the proposed LFP approach in both balanced and unbalanced networks is tested. More specifically, in the case of balanced networks, we compare the proposed method with several existing load flow methods in a 38-Bus and 33-Bus network. In the case of unbalanced networks, we compare the proposed method against the method of [21] and the NR method of OpenDSS in a 25-Bus network.

A. 38-Bus Balanced Network

Firstly, the proposed method is validated in a balanced islanded 38-Bus radial network, as presented in [14, Fig. 3]. Details about the lines, loads, and DG droop parameters are provided in [14]. The results of the proposed method are in full agreement with them of [14] since the maximum deviation of voltage magnitudes and angles between the two methods was less than 10^{-4} pu.

Table I presents some comparison results between the proposed method and some popular LFP methods that exist in literature for both islanded and grid-connected networks. More specifically, the NR, the BFS, the modified Newton-Raphson (MNR) [14], and the method of [18] are compared against the proposed approach, with respect to computation time and iteration number for a tolerance of 10^{-5} pu. It is noted that the results for NR, BFS and MNR methods are presented in [14, Table IX]. All the simulations were executed in a 64-bit laptop with processor Intel Core i5-6300HQ, 3.2GHz, 8GB RAM.

In balanced grid-connected networks, the method referred to as proposed in Table I corresponds to the implicit Z_{BUS} method in its original form [5]. It is confirmed that it presents fast convergence combined with low computation time per iteration since it needs only 6 iterations and 0.001s to converge with an accuracy of 10^{-5} pu. In islanded MG, the proposed method needs 0.03s and 31 iterations to converge. Another important thing to note is that the computation time per iteration of the proposed method in the islanded form has been increased compared to the grid-connected mode due to the iterative update of admittance matrix based on the new frequency. However, it remains significantly lower than the MNR as a result of the sparse form of the admittance matrix and the low number of variables (only the frequency) that needs to be updated. Finally, the proposed method is much faster than the method proposed in [18] for islanded MGs.

TABLE I
Performance of Various Load Flow Methods (38-Bus Balanced Network) [14]

Method	Mode	Calc. Time (s)	Iteration No.
NR method	Grid-connected	0.150	4
	Islanded	Not Applicable	Not Applicable
BFS method	Grid-connected	0.055	4
	Islanded	Not Applicable	Not Applicable
MNR method [14]	Grid-connected	Not Applicable	Not Applicable
	Islanded	0.450	8
Ref. [18]	Grid-connected	Not Applicable	Not Applicable
	Islanded	13.41	330
Proposed method	Grid-connected	0.001	6
	Islanded	0.030	31

B. 33-Bus Balanced Network

To further investigate the performance of the proposed algorithm, a comparison with the methods proposed in [12], [13] and [16] is carried out in the 33-Bus balanced network of [13, Fig. 2]. Information about the loads and lines are provided in [13], while simulations are executed for three different sets of droop gains, as referred to in [13]. The results are again in full agreement with those of [13] for all the droop sets although they are not depicted here due to space limitation. As shown in Table II, the proposed method presents by far the best computation performance for all the droop sets. Furthermore, in contrast to other methods, the proposed method remains unaffected by the variation of droop gains.

TABLE II
COMPUTATION TIME FOR VARIOUS LOAD FLOW METHODS (33-BUS BALANCED ISLANDED MG) [13]

Set of Droop Parameters	MBFS [13]	DBFS [12]	MGS [16]	Proposed Method
Droop Set 1	1.33 sec	0.82 sec	7.22 sec	0.02 sec
Droop Set 2	1.15 sec	1.08 sec	9.18 sec	0.02 sec
Droop Set 3	0.92 sec	0.44 sec	4.13 sec	0.02 sec

C. 25-Bus Unbalanced Network

To investigate the accuracy of the proposed method in unbalanced networks, we compare the proposed algorithm with the Newton-Trust Region (NTR) method [21] in the unbalanced, islanded 25-Bus network of [21, Fig. 8]. Data about the lines, loads and the droop gains of DGs are provided in [21]. All DGs are assumed to generate balanced voltages. The results of the proposed method are all in close agreement with those of [21], as shown in Table III. The proposed method spends 180 ms in order to converge with an accuracy of 10^{-5} pu. This execution time is significantly lower than the computation time of NTR. As mentioned in [11], [12], the computation time of NTR is in the range of several seconds since it involves a constrained minimization of a quadratic function, subject to a nonlinear constraint. The solution to such problems is not trivial and the computation complexity is much higher than that of the other methods.

Furthermore, we compare the proposed method with the NR method implemented in the OpenDSS software in the 25-Bus unbalanced network. A comparison is quoted in Table IV with respect to iteration number for several operation modes. As shown, when considering that DGs operate in constant PV mode, the proposed method presents faster convergence than OpenDSS, confirming the good performance of the algorithm developed in Section II-B for treating PV nodes with implicit Z_{BUS} method.

TABLE III
RESULTS OF THE PROPOSED METHOD (BOLD NUMBERS) AND METHOD IN [21] (NORMAL NUMBERS) FOR THE 25-BUS UNBALANCED ISLANDED MG

Bus No.	Phase A		Phase B		Phase C	
	Mag.	Angle	Mag.	Angle	Mag.	Angle
1	**0.9792** 0.9791	**0** 0	**0.9736** 0.9733	**-119.92** -119.93	**0.9707** 0.9707	**119.92** 119.91
2	**0.9792** 0.9791	**0** 0	**0.9736** 0.9733	**-119.92** -119.93	**0.9707** 0.9707	**119.92** 199.91
3	**0.9800** 0.9800	**0.05** 0.05	**0.9749** 0.9746	**-119.85** -119.88	**0.9720** 0.9720	**120.01** 120.09
4	**0.9812** 0.9812	**0.14** 0.14	**0.9765** 0.9762	**-119.82** -119.81	**0.9737** 0.9737	**120.11** 120.10
5	**0.9804** 0.9804	**0.14** 0.14	**0.9754** 0.9752	**-119.81** -119.81	**0.9725** 0.9725	**120.10** 120.09
6	**0.9771** 0.9770	**-0.07** -0.07	**0.9706** 0.9704	**-119.99** -119.98	**0.9673** 0.9674	**119.84** 119.83
7	**0.9766** 0.9765	**-0.14** -0.14	**0.9702** 0.9704	**-120.05** -120.04	**0.9661** 0.9662	**119.78** 119.75
8	**0.9755** 0.9754	**-0.07** -0.06	**0.9685** 0.9683	**-119.97** -119.97	**0.9650** 0.9650	**119.85** 119.82
9	**0.9813** 0.9812	**-0.21** -0.21	**0.9763** 0.9761	**-120.15** -120.14	**0.9732** 0.9732	**119.75** 119.71
10	**0.9872** 0.9871	**-0.29** -0.29	**0.9840** 0.9838	**-120.27** -120.26	**0.9817** 0.9816	**119.69** 119.67
11	**0.9911** 0.9910	**-0.34** -0.34	**0.9892** 0.9890	**-120.32** -120.33	**0.9875** 0.9874	**119.64** 119.65
12	**0.9904** 0.9903	**-0.34** -0.34	**0.9881** 0.9879	**-120.33** -120.33	**0.9864** 0.9863	**119.67** 119.66
13	**0.9975** 0.9974	**-0.42** -0.42	**0.9975** 0.9974	**-120.42** -120.42	**0.9975** 0.9974	**119.58** 119.58
14	**0.9722** 0.9722	**-0.13** -0.13	**0.9641** 0.9639	**-119.97** -119.99	**0.9591** 0.9591	**119.75** 119.73
15	**0.9706** 0.9706	**-0.13** -0.13	**0.9620** 0.9617	**-119.97** -119.98	**0.9567** 0.9568	**119.74** 199.72
16	**0.9758** 0.9757	**-0.13** -0.13	**0.9689** 0.9687	**-120.04** -120.03	**0.9650** 0.9650	**119.77** 119.75
17	**0.9713** 0.9713	**-0.13** -0.13	**0.9630** 0.9628	**-120.01** -119.99	**0.9574** 0.9575	**119.75** 119.73
18	**0.9797** 0.9797	**0.02** 0.02	**0.9752** 0.9750	**-119.94** -119.93	**0.9726** 0.9726	**119.95** 119.97
19	**0.9865** 0.9864	**-0.09** -0.09	**0.9865** 0.9864	**-120.09** -120.09	**0.9865** 0.9864	**119.91** 119.91
20	**0.9820** 0.9819	**-0.02** -0.02	**0.9792** 0.9790	**-120.00** -120.00	**0.9772** 0.9771	**119.97** 119.96
21	**0.9771** 0.9770	**0.02** 0.02	**0.9715** 0.9713	**-119.92** -119.92	**0.9681** 0.9681	**119.99** 119.98
22	**0.9756** 0.9755	**0.03** 0.03	**0.9692** 0.9689	**-119.91** -119.91	**0.9657** 0.9657	**119.99** 119.99
23	**0.9851** 0.9851	**0.22** 0.22	**0.9814** 0.9812	**-119.74** -119.75	**0.9789** 0.9789	**120.19** 120.19
24	**0.9900** 0.9900	**0.29** 0.29	**0.9874** 0.9873	**-119.70** -119.70	**0.9853** 0.9853	**120.29** 120.28
25	**1.0003** 1.0003	**0.41** 0.41	**1.0003** 1.0003	**-119.59** -119.59	**1.0003** 1.0003	**120.41** 120.41
System frequency: **f=0.9980 pu** / f=0.9980 pu						

TABLE IV
ITERATION NUMBER (25-BUS UNBALANCED NETWORK)

Mode \ Method	Proposed method	NR method of OpenDSS
Grid-Connected. Only PQ nodes	5	3
Grid-Connected. DGs in constant PV mode	16	23
Islanded. DGs in droop control	80	Not Applicable

VI. CASE STUDY INVESTIGATION

The main objective of the next case study is to investigate the robustness of the proposed algorithm in highly unbalanced and meshed islanded MGs, considering 4 different scenarios. For this purpose, the MG of Fig. 3 is considered unbalanced and the corresponding parameters are presented in Tables V and VI of Appendix B. The network consists of 24 nodes with unbalanced loads as well as 5 DGs that are uniformly distributed inside the network and operate in different operation modes.

A. Network description

One of the distinct features of the proposed LFP algorithm is its ability to handle meshed networks in contrast to BFS-based methods. The network topology of Fig. 3 is selected due to the highly meshed structure [28]. The line and load

parameters of the topology are adapted to represent the typical parameters of an LV network as depicted in Appendix B. The impedance values of cables and overhead lines are taken from [29] and [1], respectively. The size of the cables was selected based on the current limit of [30] so that none of the cables is overloaded although some of them operate close to their thermal limit.

The DGs of the investigated network have the following characteristics:

- Node 23 connects a 4-wire SG-based DG. The voltage of SG unit is not purely balanced due to the internal negative and zero sequence impedances that an SG unit inherently presents [26].
- Nodes 13 and 27 connect 4-wire EC-DGs generating balanced voltage with respect to neutral. Please note that in contrast to SG units, EC-DGs can suppress the negative and zero sequence voltage components, thus generating purely balanced voltage [25],[27].
- Nodes 2 and 22 connect 3-wire EC-DGs injecting balanced current. This case represents DGs equipped with dq-current controllers [26].

From all the above, we can conclude that the investigated 30-Bus network is a suitable test network for testing meshed LV islanded and grid-connected MGs for the following reasons: 1) It has a highly meshed structure, which usually poses extra difficulties to the solution of LFP. 2) The cables and lines present a high *R*/*X* ratio (see Appendix B), which is usually the case in LV networks. 3) The DGs include both SGs and EC-DGs. 4) The network is highly unbalanced, as shown in Appendix B. The imbalance has been further increased by connecting 3 single-phase photovoltaic units of 5KW (maximum allowable power for single-phase DGs) in phase C of nodes 17, 21 and 25. Single-phase generators are treated as negative constant power loads since they are considered to generate specified amount of power.

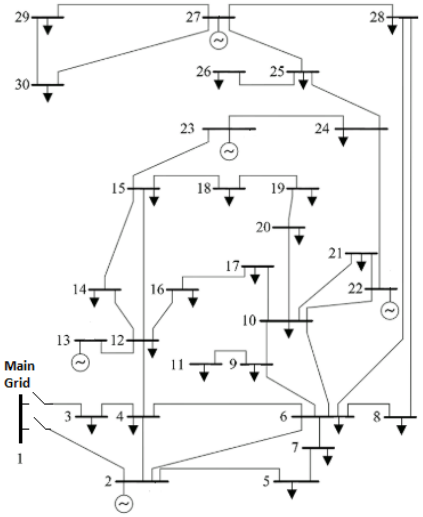

Fig. 3. 30-Bus Network operating in either grid-connected or islanded mode, with 5 DG units and 24 load nodes [28]

B. Investigated scenarios

In our analysis, we consider the following four operational scenarios:

- Scenario 1: Grid-connected mode. All DGs operate in constant PQ mode with their nominal three-phase power as shown in Table VI of Appendix B.
- Scenario 2: Islanded mode without virtual impedance. The droop gains of the DGs are given in Table V of Appendix B.
- Scenario 3: Islanded mode with virtual impedance. The values of virtual impedances of DGs are suitably selected so that the reactive power deficit due to the disconnection from the main grid is equally distributed among the DGs. More specifically, virtual impedances are selected as follows: [Z_{v2}, Z_{v13}, Z_{v22}, Z_{v23}, Z_{v27}]=[0.045j, 0.013j, 0.022j, 0.002j, 0].
- Scenario 4: Islanded mode with isochronous operation [31]. In this mode, the largest DG units (DGs 13, 23, 27) undertake the role of keeping the network frequency and their terminal voltage to pre-specified values. The other two DGs operate in constant power mode as in grid-connected scenario. The isochronous DGs generate the same amount of active power and the target frequency is set to 50 Hz. Isochronous operation is simulated using the proposed LFP approach by setting the droop gains of isochronous DGs close to zero so that the network frequency and voltage of DGs are set to the pre-specified values.

C. Results about DGs

Fig. 4 shows the active power generated by DGs for every scenario examined. The DGs in scenario 1 operate in constant PQ mode, producing a pre-specified amount of active power. After the disconnection from the main grid, all the five DGs in scenario 2 and 3 equally share the active power deficit since they have the same frequency droop gains (see K_{pi} in Appendix B). Considering scenario 4, the active power deficit is equally covered by the DGs participating in isochronous control (DGs 13, 23, 27).

Fig. 5 illustrates the reactive power variation of all DGs for scenarios 2 and 3, compared with the first grid-connected scenario. It can be observed that virtual impedances have a large influence on the reactive power of DGs, thus leading to misleading results when neglected. Furthermore, suitably selected virtual impedance values like those of Fig. 5 result in more uniform sharing of reactive power between the DGs after the disconnection from the main grid.

Finally, Fig. 6 depicts the phase-to-neutral voltage of each node for two cases: with grounding resistances 25Ω and with a perfectly grounded neutral (Z_{gri}=0 for all *i* according to Fig. 1). As shown, in both cases the DGs at nodes 13 and 27 generate a completely balanced phase voltage, validating the effectiveness of balancing equation (18). The DGs at nodes 2 and 22 are regulated to generate a balanced current resulting in a highly unbalanced voltage in these nodes due to highly unbalanced loads.

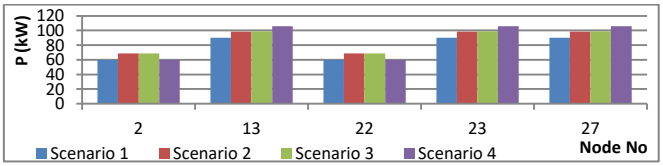

Fig. 4. Active power injection of each DG for the 4 scenarios

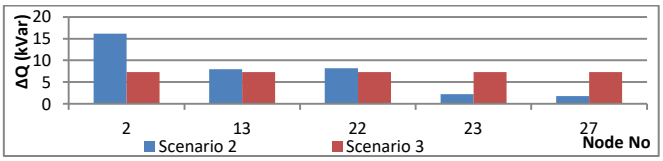

Fig. 5. Reactive power variation of each DG for scenarios 2 and 3 with respect to the first scenario

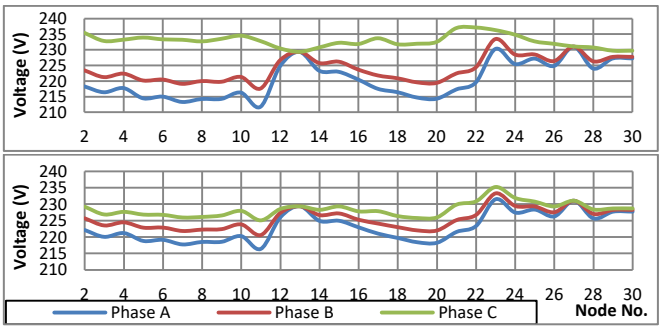

Fig. 6. Phase-to-neutral node voltages for scenario 2. From top to bottom: a) Grounding resistances equal to 25 Ω. b) Grounding resistances equal to 0 Ω.

D. *Results about the virtual slack node concept*

Fig. 7 depicts the active and reactive power of each virtual slack source (according to Fig. 1b) during the iterative process, from the 1st up to 100th iteration. As shown, after some iteration, both active and reactive powers of all phase sources are forced to zero. Thus, it is validated that the virtual slack node does not influence the operation of the network since no power is flowing through it.

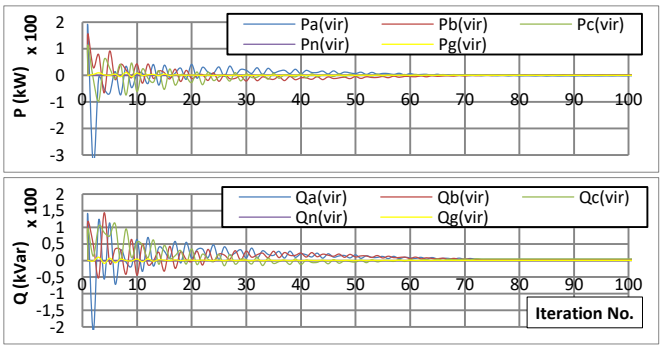

Fig. 7. Power of virtual slack sources for scenario 2 throughout the iterative process. From top to bottom: a) Active Power. b) Reactive power.

E. *Results about the neutral and grounding effects*

The effect of the neutral conductor and grounding resistances in a multigrounded LV network is highlighted in the following paragraphs using the proposed LFP approach. Two different operational conditions of the network are investigated: 1) steady-state analysis in normal operation, 2) steady-state analysis with an open neutral conductor. Regarding the operational mode of the network and DGs, scenario 2 is adopted for all cases.

1) *Steady-state analysis in normal operation*

The perfectly grounded neutral is an approximate assumption that is adopted by many papers, e.g., [11]-[18], leading to misleading results in unbalanced LV networks. As shown in Fig. 6, the calculated imbalance of the network is significantly reduced when the neutral conductor is assumed to have a zero voltage along the network. In reality, the return current causes a voltage drop in the neutral conductor, affecting the phase-to-neutral voltage of all phases. It also increases the losses of the network. Thus, in unbalanced LV networks, the explicit representation of neutral and grounding conductors is necessary.

Fig. 8 depicts the neutral-to-earth voltages of each node, considering different grounding resistances. As shown, for higher values of grounding resistances, the common mode noise limit for sensitive electronic equipment [4] [32] is exceeded in some nodes. On the other hand, low values of grounding resistances increase the earth leakage currents, which can be harmful for underground metal facilities such as pipes and steelwork of buildings [3].

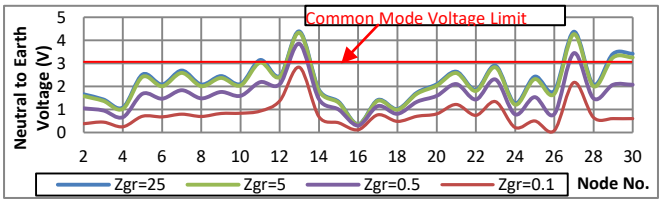

Fig. 8. Neutral-to-earth node voltages for scenario 2 considering different grounding resistances

2) *Steady-state analysis with an open neutral conductor*

In the next example, we investigate the adverse effect of an open neutral conductor in four-wire LV networks. The open neutral condition, while not frequent, can cause significant damage to a customer's electrical equipment and endanger the customer's safety. It is because the return currents flow through the high grounding impedance instead of neutral conductor, causing a significant neutral-to-earth shifting [33].

In our example, we considered an open neutral conductor between nodes 9 and 11 with grounding resistance Z_{gr}=3 Ω. Fig. 9 depicts the phase-to-neutral as well as the neutral-to-earth voltage of each node. Two adverse effects are observed in node 11. First, there is a neutral-to-earth rise ($V_{n\text{-}g}$) to around 37V. Second, the phase-to-neutral voltage of the most loading phase ($V_{a\text{-}n}$) falls to around 178V, while the less loading phase ($V_{c\text{-}n}$) rises to around 262V. For higher grounding resistances, the problem could be worse. Open neutral effects are usually not detected by the overcurrent relays, and the network can operate in this condition for a long time.

With the existing load flow methods for islanded MGs so far, all the above-mentioned effects (open neutral, common mode noise and leakage currents, safety issues, etc) remain unexplored since the neutral and grounding are either neglected or hidden through Kron's reduction. This research gap is addressed with the proposed load flow approach.

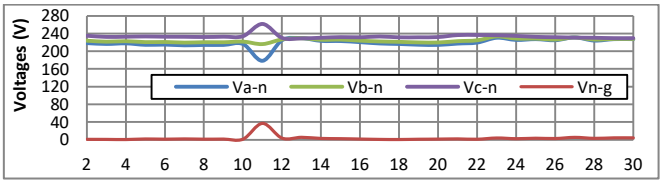

Fig. 9. Phase-to-neutral and neutral-to-earth node voltages for scenario 2 during an open neutral conductor between the nodes 9 and 11

VII. Conclusion

This paper presented an exact algorithm for solving the unbalanced LFP in grid-connected LV networks. The algorithm is based on the implicit Z_{BUS} method and has low computation time and high robustness. The method was subsequently modified to solve the LFP in islanded balanced and unbalanced MGs, considering different operation modes of DGs. An additional algorithm was also proposed for integrating the virtual impedance control concept of DGs into the LFP.

A summary of the main contributions of the proposed load flow algorithm is as follows.

✓ It can be readily applied in highly mesh and highly unbalanced networks with high *R*/*X* ratios.

✓ It presents a low computation burden since it does not need any Jacobian matrix inversion.

✓ It overcomes the limitation of conventional implicit Z_{BUS} methods to handle networks with PV nodes.

✓ It proposes a method to solve the LFP in balanced islanded MGs. The method is also applicable with other LFP solvers (e.g NR, BFS, GS).

✓ To the author's knowledge, this is the first time the LFP of an islanded MG is solved in such a precise way by explicitly considering all the five conductors, including neutral and grounding, and mutual line impedances. Thus, the analysis of several power quality and safety issues (e.g., open neutral effect, ground fault and leakage currents, ground potential rise, sensitivity of ground fault relays, etc.) is enabled.

✓ The virtual impedance control concept, which is usually ignored, was also considered for more precise results.

Appendix A

A1. Acceleration Factor of Frequency:

Using a multiplication factor in (16b), (A1) is derived and the convergence of the algorithm can become faster:

$$f^{k+1} = f^{k} + acc1 \cdot df^{k} \qquad \text{(A1)}$$

where *acc1* is an acceleration factor with typical values between 0.5 and 1.

A2. Acceleration Factor of Reactive Power:

Equation (A2) estimates the reactive power of DG *i* at the next iteration *k*+1 also considering the reactive power of the previous iteration *k*. Through a suitable selection of the acceleration factor *acc2*, the convergence of the algorithm can be improved. Typical values for *acc2* are between 0.2 and 1. It is reminded that Q_{Gi}, in the right side of (A2) is calculated from (13b), from the voltage values of the last iteration.

$$Q_{Gi}^{k+1} = Q_{Gi}^{k} + acc2 \cdot (Q_{Gi} - Q_{Gi}^{k}) \qquad \text{(A2)}$$

Appendix B

TABLE V
Parameters of Unbalanced Network of Fig. 3

Self Impedance of the lines	See Table VI of Appendix B
Mutual-Reactance of the lines	0.1 mH/km
Line lengths	See Table VI of Appendix B
Loads of PQ nodes (P_A,P_B, P_C)	See Table VI of Appendix B
K_{Pi} (*i*=2, 13, 22, 23, 27)	$5 \cdot 10^{-7}$ (Hz/W)
K_{Qi} (*i*=2, 13, 22, 23, 27)	$2 \cdot 10^{-4}$ (V/VAR)
Ground resistances	25 Ohm (unless otherwise stated)

TABLE VI
Line and Load Parameters of Unbalanced Network of Fig. 3

Bus No.	To Bus	Type of line	Size (mm^2)	Length (m)	R + X·j (in Ohm/km at 50Hz)	Phase Load (KW)*		
						A	B	C
1	2	Cable	35	100	0.668+0.091·j	-	-	-
	3	Cable	35	50	0.668+0.091·j			
2	4	Cable	35	50	0.668+0.091·j	60kW, 40kVAR		
	5	Cable	35	100	0.668+0.091·j			
	6	Cable	35	150	0.668+0.091·j			
3	4	Cable	35	50	0.668+0.091·j	7	6	5
4	6	Cable	35	100	0.668+0.091·j	7	6	5
	12	Cable	35	100	0.668+0.091·j			
5	7	Cable	16	50	1.47+0.0993·j	7	6	5
6	7	Cable	16	50	1.47+0.0993·j	7	6	5
	8	Cable	35	50	0.668+0.091·j			
	9	Cable	35	50	0.668+0.091·j			
	10	Cable	35	100	0.668+0.091·j			
	28	Overhead	35	500	0.576+0.397·j			
7	-	-	-	-	-	7	6	5
8	28	Overhead	35	500	0.576+0.397·j	7	6	5
9	10	Cable	35	50	0.668+0.091·j	7	6	5
	11	Cable	6	50	3.93+0.113·j			
10	17	Cable	35	50	0.668+0.091·j	7	6	5
	20	Cable	35	100	0.668+0.091·j			
	21	Cable	35	100	0.668+0.091·j			
	22	Cable	35	50	0.668+0.091·j			
11	-	-	-	-	-	7	6	5
12	13	Cable	95	50	0.247+0.0833·j	7	6	5
	14	Cable	35	50	0.668+0.091·j			
	15	Cable	35	150	0.668+0.091·j			
	16	Cable	35	50	0.668+0.091·j			
13	-	-	-	-	-	90kW, 70kVAR		
14	15	Cable	35	100	0.668+0.091·j	7	6	5
15	18	Cable	16	50	1.47+0.0993·j	7	6	5
	23	Cable	35	100	0.668+0.091·j			
16	17	Cable	35	50	0.668+0.091·j	7	6	5
17	-	-	-		-	7	6	5**
18	19	Cable	35	50	0.668+0.091·j	7	6	5
19	20	Cable	35	50	0.668+0.091·j	7	6	5
20	-	-	-	-	-	7	6	5
21	22	Cable	35	50	0.668+0.091·j	7	6	5**
22	24	Cable	35	150	0.668+0.091·j	60kW, 40kVAR		
23	24	Cable	35	100	0.668+0.091·j	90kW, 70kVAR		
24	25	Cable	35	100	0.668+0.091·j	7	6	5
25	26	Cable	6	50	3.93+0.113·j	7	6	5**
	27	Cable	35	50	0.668+0.091·j			
26	-	-	-		-	7	6	5
27	28	Overhead	35	100	0.576+0.397·j	90kW, 70kVAR		
	29	Cable	35	150	0.668+0.091·j			
	30	Cable	35	150	0.668+0.091·j			
28	-	-	-	-	-	7	6	5
29	30	Cable	35	50	0.668+0.091·j	7	6	5
30	-	-	-	-	-	7	6	5

*All loads operate with cosφ=0.8. **A single-phase photovoltaic of 5KW is connected in phase C of node 17, 21, 25 and is not included in the Table.

REFERENCES

[1] E. E. Pompodakis, I. A. Drougakis, I. S. Lelis, M. Alexiadis, "Photovoltaic systems in low-voltage networks and overvoltage correction with reactive power control," *IET Renew. Power Gener.*, vol. 10, no. 3, 410–417, 2016.

[2] "IEEE Std. 142–2007 (Revision of IEEE Std. 142-1991)", *IEEE Recommended Practice for Grounding of Industrial and Commercial Power Systems*, 2007.

[3] T.-H. Chen, W.-C. Yang, "Analysis of multi-grounded four-wire distribution systems considering the neutral grounding", IEEE Trans. Power Deliv., vol. 16, no. 4, pp. 710–717, 2001.

[4] M.J.E. Alam, et al., "A three-phase power flow approach for integrated 3-wire MV and 4-wire multigrounded LV networks with rooftop solar PV", *IEEE Trans. Power Syst.*, vol. 28, no. 2, pp. 1728–1737, 2013.

[5] T. H. Chen *et al.*, "Distribution system power flow analysis–A rigid approach," *IEEE Trans. Power Del.*, vol. 6, no. 3, pp.1146–1152, 1991.

[6] T. Zhao *et al.*, "Convergence analysis of implicit Z-bus power flow method for general distribution networks with distributed generators," *IET Gener. Transm. Distrib.*, vol. 10, no. 2, pp. 412–420, 2016.

[7] R. M. Ciric *et al.*, "Power flow in four-wire distribution networks–general approach", *IEEE Trans. Power Syst.*, vol. 18, no. 4, pp. 1283–1290, 2003.

[8] E. Demirok *et al.*, "Three-phase unbalanced load flow tool for distribution networks," 2nd Work. Integr. of Solar Power Syst., 2012.

[9] D. R. R. Penido *et al.*, "Three-phase power flow based on four-conductor current injection method for unbalanced distribution networks," *IEEE Trans. Power Syst.*, vol. 23, no. 2, pp. 494–503, 2008.

[10] N. C. Yang, "Three-phase power flow calculations using direct Z_{BUS} method for large-scale unbalanced distribution networks," *IET Gener. Transm. Distrib.*, vol. 10, pp. 1048–1055, 2016.

[11] M. Nassar, M. Salama, "A novel branch based power flow algorithm for islanded AC microgrids," *Elect. Power Syst. Res.*, 51–62, 2017.

[12] G. Diaz, J. Gómez-Aleixandre, J. Coto, "Direct backward/forward sweep algorithm for solving load power flows in AC droop-regulated microgrids," *IEEE Trans. Smart Grid*, vol. 7, no. 5, pp. 2208–2217, 2016.

[13] F. Hameed, M.A. Hosani, H.H. Zeineldin, "A Modified Backward/Forward Sweep Load Flow Method for Islanded Radial Microgrids", *IEEE Transactions on Smart Grid*, vol. 10, no. 1, pp. 910–918, 2019.

[14] F. Mumtaz *et al.*, "A novel approach to solve power flow for islanded microgrids using modified newton Raphson with droop control of DG," *IEEE Trans. Sustain. Energy*, vol. 7, no. 2, pp. 493–503, 2016.

[15] L. Rese, A. Simões Costa, A. S. Silva, "A modified load flow algorithm for microgrids operating in islanded mode," *IEEE Innov. Smart Grid Tech.*, Latin America (ISGT LA), 2013.

[16] F. Mumtaz *et al.*, "A simple and accurate approach to solve the power flow for balanced islanded microgrids", *in 15th Int. Conf. Environ. Electr. Eng.*, Rome, pp. 1852–1856, 2015.

[17] M. H. Moradi *et al.*, "Power flow analysis in islanded Micro-Grids via modeling different operational modes of DGs: A review and a new approach," *Renew. Sustain. Energy Rev.*, 248–262,2017.

[18] G. C. Kryonidis *et al.*, "Power flow of islanded AC microgrids: Revisited", *IEEE Trans. Smart Grid*, vol. 9, no 4, pp. 3903–3905, 2018.

[19] M.Z. Kamh, R. Iravani, "A sequence frame-based distributed slack bus model for energy management of active distribution networks," *IEEE Trans. Smart Grid*, vol. 3, no. 2, pp. 828–836, 2012.

[20] M.A. Elizondo, F.K. Tuffner, K.P. Schneider, "Three-phase unbalanced transient dynamics and power flow for modeling distribution systems with synchronous machines", *IEEE Trans. Power Syst.*, vol. 31, no. 1, pp. 105–115, 2016.

[21] M. M. A. Abdelaziz *et al.*, "A novel and generalized three-phase power flow algorithm for islanded microgrids using a Newton trust region method," *IEEE Trans. Power Syst.*, Vol. 28, No 1, pp. 190–201, 2013.

[22] C. Li *et al.*, "Power flow analysis algorithm for islanded LV microgrids including distributed generator units with droop control and virtual impedance loop", *Applied Power Electr. Conf. and Expos.*, 2014.

[23] C. Li *et al.*, "Power Flow Analysis for Low-voltage AC and DC Microgrids Considering Droop Control and Virtual Impedance", *IEEE Trans. Smart Grid*, vol. 8, no. 6, pp. 2754–2764, Nov. 2017.

[24] G. C. Kryonidis et al., "A simulation tool for extended distribution grids with controlled distributed generation," in *PowerTech, 2015 IEEE Eindhoven*, June 2015, pp. 1–6.

[25] X. Zhou *et al.*, "Four-leg converters with improved common current sharing and selective voltage-quality enhancement for islanded microgrids," *IEEE Trans. Power Del.*, vol. 31, no. 2, pp. 522–531, Apr. 2016.

[26] M.Z. Kamh, R. Iravani, "Unbalanced model and power-flow analysis of microgrids and active distribution systems," *IEEE Trans. Power Del.*, vol. 25, no. 4, pp. 2851–2858, 2010.

[27] H. Karimi, A. Yazdani, R. Iravani, "Robust control of an autonomous four wire electronically-coupled distributed generation unit," *IEEE Trans. Power Del.*, vol. 26, no. 1, pp. 455–466, 2011.

[28] J.Oliver, T. Kipouros, A. MarkSavill, "Electrical Power Grid Network Optimisation by Evolutionary Computing", *Procedia Computer Science*, Vol. 29, 1948–1958, 2014.

[29] Fujikura Federal Cables Sdn. Bhd. LOW VOLTAGE POWER CABLE Technical Data A.C. Resistance, Reactance and Impedance Rated Voltage : 600/1000V, Retrieved April 13, 2019, from: http://ffcpg.com.my/portal/Products.nsf/2d248e16d8d12df4825719b00301d50/5801a1bfde86e113482577e40009d126/$FILE/LV TD.pdf

[30] Fujikura Federal Cables Sdn. Bhd. LOW VOLTAGE POWER CABLE Technical Data Current Currying Capacity Rated Voltage : 600/1000V, Retrieved April 13, 2019, from: http://www.ffcpg.com.my/portal/Products.nsf/32d248e16d8d12df4825719b00301d50/5801a1bfde86e113482577e40009d126/$FILE/LV%20CCC.pdf

[31] A. Mohd et al., "Isochronous load sharing and control for inverter-based distributed generation," *International Conference on Clean Electrical Power*, pp.324–329, June 2009.

[32] T. M. Gruzs, "A survey of neutral currents in three-phase computer power systems," *IEEE Trans. Ind. Appl.*, vol. 26, no. 4, pp. 719–725, 1990.

[33] C. D. Halevidis, E. I. Koufakis, "Power flow in PME distribution systems during an open neutral condition", *IEEE Trans. Power Syst.*, vol. 28, no. 2, pp. 1083–1092, 2013.

Evangelos E. Pompodakis received the Diploma and Master degrees from the School of Electrical and Computer Engineering at the Aristotle University of Thessaloniki, Greece and the Technical University of Kaiserslautern, Germany in 2011 and 2015 respectively. Between 2015 and 2017 he worked in several positions of Energy sector in Greece. He is currently pursuing a Ph. D. degree in Aristotle University of Thessaloniki. His research interests include, power flow analysis, distributed generation and storage, power converters, smart grids operation and control.

Georgios C. Kryonidis (S'12-M'18) received the Dipl. Eng. and Ph. D. degrees from the School of Electrical and Computer Engineering at the Aristotle University of Thessaloniki, Greece, in 2013 and 2018, respectively. He is currently a Research Fellow with the School of Electrical and Computer Engineering, Aristotle University of Thessaloniki. His research interests include, distributed generation and storage, renewable energy sources, and smart grids operation and control.

Minas C. Alexiadis was born in Thessaloniki, Greece, in July 1969. He received the Dipl. Eng. Degree (1994) and the Ph.D. Degree (2003) from the School of Electrical Engineering at the Aristotle University of Thessaloniki (AUTh), Greece. He is currently an Assistant Professor at the same School. He has been working on Greek or European research projects since the late 90s. His research fields include renewable energy sources and distributed generation, artificial intelligence applications in power systems, electric vehicles, CO2 mitigation, classification of electricity consumers, optimal energy design for freeways and tunnels, smart lighting systems etc. He is also the Faculty Advisor of Aristotle University Racing Team Electric (Aristurtle) which is currently No 41 in the World Ranking List of Formula Student Electric.